Comparison of time-gated surface-enhanced raman spectroscopy (TG-SERS) and classical SERS based monitoring of Escherichia coli cultivation samples

Kögler, Martin

2018

Kögler , M , Paul , A , Anane , E , Birkholz , M , Bunker , A , Viitala , T , Maiwald , M , Junne , S & Neubauer , P 2018 , ' Comparison of time-gated surface-enhanced raman spectroscopy (TG-SERS) and classical SERS based monitoring of Escherichia coli cultivation samples ' , Biotechnology Progress , vol. 34 , no. 6 , pp. 1533-1542 . https://doi.org/10.1002/btpr.2665

http://hdl.handle.net/10138/327074
https://doi.org/10.1002/btpr.2665

unspecified
acceptedVersion

Comparison of time-gated surface-enhanced Raman spectroscopy (TG-SERS) and classical SERS based monitoring of *Escherichia coli* cultivation samples

Martin Kögler[1,3], Andrea Paul[2], Emmanuel Anane[1], Mario Birkholz[4], Alex Bunker[3], Tapani Viitala[3], Michael Maiwald[2], Stefan Junne[1] and Peter Neubauer[1]*

[1] Chair of Bioprocess Engineering, Department of Biotechnology, Technische Universität Berlin, Ackerstr. 76 ACK24, D-13355 Berlin, Germany

[2] Bundesanstalt für Materialforschung und -prüfung (BAM), Richard-Willstätter-Straße 11, D-12489 Berlin, Germany

[3] Drug Research Program, Faculty of Pharmacy, Division of Pharmaceutical Biosciences, University of Helsinki, P.O. Box 56, 00014 Helsinki, Finland

[4] IHP, Im Technologiepark 25, 15236 Frankfurt (Oder), Germany

*Corresponding Author: E-mail: peter.neubauer@tu-berlin.de, phone: +49 30 314 72573

ABSTRACT

The application of Raman spectroscopy as a monitoring technique for bioprocesses is severely limited by a large background signal originating from fluorescing compounds in the culture media. Here we compare time-gated Raman (TG-Raman)-, continuous wave NIR-process Raman (NIR-Raman) and continuous wave micro-Raman (micro-Raman) approaches in combination with surface enhanced Raman spectroscopy (SERS) for their potential to overcome this limit. For that purpose, we monitored metabolite concentrations of *Escherichia coli* bioreactor cultivations in cell-free supernatant samples. We investigated concentration transients of glucose, acetate, AMP and cAMP at alternating substrate availability, from deficiency to excess. Raman and SERS signals were compared to off-line metabolite analysis of carbohydrates, carboxylic acids and nucleotides. Results demonstrate that SERS, in almost all cases, led to a higher number of identifiable signals and better resolved spectra. Spectra derived from the TG-Raman were comparable to those of micro-Raman resulting in well-discernable Raman peaks, which allowed for the identification of a higher number of compounds. In contrast, NIR-Raman provided a superior performance for the quantitative evaluation of analytes, both with and without SERS nanoparticles when using multivariate data analysis.

Keywords: time-gated Raman (TG-Raman); surface-enhanced Raman spectroscopy (SERS); multivariate data analysis; metabolite quantification; *Escherichia coli*

1. Introduction

Raman spectroscopy is a versatile technique for simultaneous concentration monitoring of various target compounds in the liquid phase of biotechnological processes, in particular substrate and side product accumulation, or recently glycolysation[1]. However, the broad application of Raman spectroscopy for the detection of compounds in the liquid phase upstream of microbial processes is mainly restricted to research purposes so far, although, in comparison to IR spectroscopic approaches, Raman bands of most analytes exhibit no interference with vibrations from water molecules[2–4]. This is due to the basic drawback of Raman spectroscopy, i.e. data treatment and confidence limits are often not really optimized[5], and a high fluorescence background causes high threshold values for most analytes in biological samples[6,7], and thus a low sensitivity[8]. In addition, the fluorescence background often dominates the Raman spectrum even when using common near-infrared (NIR) laser excitation sources[9,10].

Several approaches have been developed to overcome impacts of fluorescence background, e.g. shifted-excitation Raman difference spectroscopy (SERDS), coherent anti-Stokes Raman spectroscopy (CARS), resonance Raman spectroscopy (RR), surface-enhanced Raman spectroscopy (SERS) and time-gated (TG) Raman spectroscopy. SERDS is based on the difference spectrum of two identically recorded spectra, which are separated typically by the full-width-at-half-maximum (FWHM). When applying this, Raman bands are shifted by the FWHM, whereas the broad fluorescence remains unchanged. Fluorescence background noise is supressed when the two Raman spectra are subtracted from each other[11,12]. CARS involves the measurement of anti-Stokes shifted Raman and requires two pulsed laser excitation sources. It provides a non-linear stimulated Raman emission at a shorter wavelength than the excitation laser wavelength. This wavelength has a larger distance from the maximum induced fluorescence in a sample[13,14]. RR combined with a picosecond (ps) short-pulsed infrared excitation laser source is capable of separating the Raman signal from fluorescence[15]. SERDS, CARS and RR have good prospects, but are currently academic approaches. In contrary to these approaches, SERS and TG-Raman showed convincing signal enhancement and fluorescence suppression, and are thus in the focus of this work.

SERS uses the enhancement of the Raman-signal by a factor of $10^4 - 10^{10}$ near metallic roughened surfaces, electrodes or on colloidal metal nanoparticles. The effect is related to the excitation of localized surface plasmons and enables a single-molecule detection[16,17]. In addition, the strong enhancement of the Raman signal with SERS quenches the fluorescence background, which was confirmed earlier with the Gersten–Nitzan model and the Mie scattering theory[8,9,18,19]. Despite the high potential of SERS for signal enhancement, the practical implementation is still a challenge. Recently, the focus lies on the improvement of reproducibility of real-time measurements under process conditions[20,21]. Nevertheless, the increasing demand for parallel cultivations during process development and in the upstream part of bioprocesses, and the availability of automated liquid handling systems for sample treatment, allow the application of a more sophisticated sample treatment, if benefits of higher specificity and the utilization of one single measurement device instead of multiple probes compensate the common drawbacks of off-line measurements.

While SERS reduces the fluorescence background by enhancing the Raman signal, time-gating "gates out" not only the fluorescence, but also other disturbing signals like cosmic rays or room light [6,22]. The TG-Raman approach has reached the stage of a commercially available solution enabling routine process measurements. The set-up utilizes the synchronization of a pulsed laser excitation in a 100 ps-time regime with a complementary metal–oxide–semiconductor (CMOS) single-photon avalanche diode (SPAD)-detector in a compact system, as opposed to the more common charge-coupled device (CCD) detectors[6,23].

We therefore decided to utilize TG-Raman and two continuous wave (CW) Raman approaches with and without SERS and compared their potential to analyse cell-free supernatant samples of an *Escherichia coli* cultivation. The conventional approaches comprise a CW laser Raman process spectrometer with NIR excitation at 785 nm and a confocal CW-microscopic set-up at 633 nm, which is considered to be the most precise instrument regarding spectral resolution with high spatial accuracy as a standard to perform SERS as a reference (cf. section 2.3). For SERS measurements, we used commercially available inexpensive silver nanoparticles (Ag NPs), which are known to be stable over a long time with good signal enhancement and uniformity in particle size.

We aimed at the quantification of glucose as main carbon source, acetate as main side metabolite, and selected amino acid and nucleotide concentrations with all three set-ups. These shall represent metabolites, which are of interest to monitor a bacterial cultivation process. The spectra were evaluated by both, a univariate and multivariate data analysis (MVDA). Enzymatic analysis and high-performance liquid chromatography (HPLC) were used as reference data for calibration and validation of the chemometric approaches.

The following topics were addressed: (i) which experimental set-up is best suited for a comprehensive analysis of the analytes of interest, (ii) to what extent does SERS offer benefits over conventional Raman, and (iii) which specifications have to be met for efficient bioprocess monitoring by Raman spectroscopy?

2. Materials and Methods

2.1 Chemicals

Commercial silver nanoparticles (Ag NPs) of a size of 40 nm, measured with transmission electron microscopy in a suspension of 0.02 mg mL^{-1} in aqueous buffer, containing sodium citrate as stabilizers (Sigma-Aldrich, St. Louis, MO) were applied for the SERS studies. Prior to measurements, the stock solution was centrifuged (CT15RE from VWR, Radnor, PA) at 4,000 rpm / 1,610 x g for 4 min, subsequently followed by a removal of the supernatant to reach a final concentration of about 2.8 $g \cdot L^{-1}$. The effect of different size, shape and enhancement material was tested in our earlier studies, in which these Ag NPs showed good performance at different wavelengths with different spectroscopic set-ups [24,25]. The nanotoxicity of Ag NPs on *E. coli* cells was described elsewhere [26], which should not be relevant, as the assay was exclusively used during measurements.

2.2 Microbial cultivation

A batch and subsequent fed-batch cultivation of wild type *E. coli* W3110 in a 3.7 L stirred-tank bioreactor with a pulse-based feeding profile was applied to achieve different concentrations of glucose and other metabolites, including those typically appearing under conditions of overflow metabolism.

The batch phase was started with 2 L mineral salt medium, containing (per L): 2 g Na_2SO_4, 2.468 g $(NH_4)_2SO_4$, 0.5 g NH_4Cl, 14.6 g K_2HPO_4, 3.6 g $NaH_2PO_4 \times 2H_2O$, 1 g $(NH_4)_2$-H-citrate and 1 mL of antifoam (Antifoam 204, Sigma Aldrich GmbH, Darmstadt, Germany). Before inoculation, the medium was supplemented with (per L) 2 mL of trace elements solution, 2 mL of $MgSO_4$ solution (1.0 M), and with 5 g of glucose for the batch phase. The trace element solution comprised (per L): 0.5 g $CaCl_2 \times 2H_2O$, 0.18 g $ZnSO_4 \times 7H_2O$, 0.1 g $MnSO_4 \times H_2O$, 20.1 g Na-EDTA, 16.7g $FeCl_3 \times 6H_2O$, 0.16 g $CuSO_4 \times 5H_2O$, and 0.18 g $CoCl_2 \times 6H_2O$. During cultivation, the temperature was maintained at 37 °C and the pH was controlled at 7.0 by automatic titration with a solution of 25% NH_4OH. After 10 hours of batch cultivation, a sudden rise in the dissolved oxygen profile appeared while glucose depleted. An exponential feeding was subsequently implemented to maintain the achieve a specific growth rate of 0.3 h^{-1}. The feed solution contained (per L) 8 mL of trace elements solution, mineral salts (same concentration as in the batch phase) and 400 g of glucose. In order to achieve the heterogeneous environment required for the secretion of important metabolites in *E. coli*, the feed was supplied intermittently as pulses, and samples were drawn at the pulsing times. Cell-free supernatant samples were taken through a membrane filter (pore-size of 0.22 µm), with which the supernatant was directly separated from cells during sampling. The samples were frozen and stored at -80° C prior to further analysis. All reference measurements were conducted within a close time span to the Raman spectroscopy measurements.

2.3 Raman spectroscopy analysis

2.3.1 Raman microscopy (micro-Raman)

A confocal Raman microscope (InVia from Renishaw, Wotton-under-Edge, UK) [27] was used encompassing a CCD-detector, which was temperature-controlled at -70°C during measurements, and a CW He-Ne laser with an excitation at λ_{exc}= 633 nm, a laser power of 10 mW at lens (N Plan EPI from Leica, Wetzlar, Germany) with a magnification factor of 20x and numerical aperture (NA) of 0.4. The spectral acquisition time was set to 10 s. An average of 5 captures was considered with a manual cosmic ray removal. The spectral resolution of the InVia Raman microscope was 0.3 cm^{-1} at FWHM.

2.3.2 NIR Raman spectrometer (NIR-Raman)

A commercially available process Raman spectrometer RXN1 (Kaiser Optical Systems, Ann Arbor, MI)[28] was used, which was equipped with a temperature-controlled CCD detector at -40° C and a CW-laser excitation at λ_{exc}= 785 nm at a laser power of 135 mW at a non-immersion Raman MR process probe (NA = 0.29). The spectral acquisition with NIR-Raman was performed with an integration time of 20 s. An average of 5 captures was considered, which reduced cosmic ray disturbances. The spectral resolution of the RXN1 spectrometer was 4 cm^{-1} (FWHM).

2.3.3 Time-gated Raman (TG)

For this study, a prototype system set-up of a time-gated Raman process-spectrometer TGM1 (TimeGate Instruments, Oulu, Finland) equipped with a state-of-the-art non-cooled SPAD detector with a 100 ps pulsed Nd:YVO_4 laser at λ_{exc}= 532 nm was used. A standard laboratory Raman probe BWTek RPB 532 (B&W Tek, Newark, DE) with an approximate average laser power of 30 mW and NA of 0.22 at the sample focal point was applied. No cosmic ray removal was necessary due to the fast gating duty cycle of the measurement principle. The time-gating principle was described elsewhere [6,9,23]. SERS was conducted with the same spectral range, laser power, repetitions and temporal settings. Even though a single measurement at the temporal position of high intensity Raman or SERS signal was recorded in about 1.5 seconds, repetitions in temporal direction were necessary (15 min. of total collection time) to achieve a well-resolved overall spectrum for one sample (cf. Fig. S1) with sufficient signal-to-noise ratio[29]. However, for practical reasons, each TG-spectrometer is equipped with individually adjustable delay-settings, which results in a temporal off-set from t = 0 (launch of a laser pulse), as shown in the results of the raw-data (cf. Fig. S1). The temporal window used in this study was set to cover the Raman and SERS signal captures between t = 1.2 – 2.1 ns. The spectral resolution of the TG-system was 10 cm^{-1} (FWHM).

2.4 Sample preparation & measurement procedure

Prior to the analyses, a wavelength calibration was performed for all three Raman spectrometers. Laser and detectors were temperature-stabilized. Measurements were performed with an in-house developed anodized aluminum microwell plate with a cavity volume of 20 µL. At first, 3 µL of samples were filled into the wells. Raman spectra were recorded subsequently. In a next step, 3 µL of concentrated Ag NPs solution was added without mixing into the sample. Subsequent SERS measurements were performed after focussing beneath the liquid surface of each sample, while adjusting to the maximum Raman/SERS intensity at each spectrometer set-up (cf. Fig. 1 and Fig. 2). All spectra were taken immediately after pipetting the supernatant samples into the wells. Repeated SERS measurements were performed sequentially right after each Raman measurement by adding Ag NPs on top of the sample. Fig. 1 shows the settings used for the different measurements.

2.5 Reference analysis

The glucose concentration was enzymatically determined with the glucose hexokinase FS kit (DiaSys Diagnostics, Holzheim, Germany) following the supplier's instructions. Carbohydrates, short chain carboxylic acids and ethanol were quantified with a refractive index detector on a HPLC-system (1200 series system, Agilent, Waldbronn, Germany), amino acids were quantified with a fluorescence detector on a HPLC (1260 series system, Agilent) using pre-column derivatization with o-phthal-dialdehyde [30]. Nucleotides were quantified with a diode-array detector (1200 series system, Agilent). For separation, a Supelcosil TM LC-18T column (150 mm × 4.6 mm I.D., 3 µm particle size) connected to a guard column cartridge (particle size of 5 µm) was applied (both Supelco, Bellefonte, PA). Chromatographic conditions were set as described elsewhere with a flow rate of 1.0 $mL \cdot min^{-1}$ [31]. Repeated Raman and SERS reference measurements for most media compounds were performed with a concentration range from close to the limit of detection up to the highest available concentration (cf. Fig. S3 and S4).

2.6 Spectral data processing

In order to achieve time-gated Raman spectra, a post-processing was performed using the instruments' post-processing software[32].

The TG-Raman raw measurement data provides a three dimensional data cube, i.e., intensity versus Raman signal wavenumbers versus time delay information. The latter exhibits the Raman signal as function of the time delay in several nanoseconds. The time region with a typical time span of 0.5 – 5.5 ns, in which the Raman signals arises shortly before the fluorescence signal, is of great importance. Typical 3D raw-data cubes are depicted in the supplementary information (Figure S1).

Further analysis was performed with OriginPro (V. 2016, OriginLab, Northampton, MA). MVDA of Raman and SERS in general started with principal component analysis (PCA) for initial data inspection followed by partial least squares regression (PLSR) of mean-centered data with the software The Unscrambler® X (V.10.4. CAMO Software, Oslo, Norway). Prior to regression analysis, TG spectra were baseline-corrected and unit vector normalized, whereas for both micro-Raman and NIR-Raman spectra, a Savitzky-Golay derivative over 21 spectral data points using a second order polynomial followed by unit vector normalization was applied. The latter allows for a quantitative comparison of data retrieved at different experimental periods and thus was applied as a final step for all spectral data. In case of unit vector normalization, each sample vector is divided by its own size. The normalized samples have a length (norm) of "1" and differ only with respect to their direction.

The off-line derived data for optical density (OD), acetate, glucose, amino acid and nucleotide, i.e., adenosine monophosphate (AMP) and cyclic AMP (cAMP) concentrations were included as response variables (y) for calibration of the PLSR models, and the so-called fingerprint region of each spectroscopic data set after the described mathematical pre-treatment as x variables. The resulting root mean square errors of calibration (RMSEC) and validation (RMSECV) can be compared as figures of merit among various Raman measurements for the same analyte. The validation was performed as internal (full) cross validation for model development. The optimal rank A (number of factors, latent variables) is determined based on prediction of kept-out objects (samples) from the individual models by cross validation. Moreover, the approximate uncertainty variance of the PLS regression coefficients

B can be estimated by jack-knifing according to Martens and Martens[33]. As a rough significance test, a Student's t-test is performed for each element in *B* relative to the square root of its estimated uncertainty variance, giving the significance level for each parameter.

In addition, for both micro-Raman and NIR-Raman spectra, pseudo-external validation (RMSEP) was performed using repeated measurements of different aliquots from samples of the dynamic cultivation. To assess prediction uncertainties of unknown samples including biological variation, the investigation of several batch cultivations will be necessary. Such experiments would be the next step after having identified the optimal Raman technique for the analytes of interest, but are, however, beyond the aim of this study.

3. Results and Discussion

The aim of this study was to compare the potential of different suitable Raman and SERS approaches for both, the spectral identification and quantification of relevant compounds in cell-free supernatants, namely NIR-Raman at 785 nm with continuous excitation and TG-Raman at 532 nm with pulsed excitation. The micro-Raman was used as reference at a continuous excitation of 633 nm. Measurements were performed with supernatant samples of an *E. coli* cultivation with mineral salt medium. These cultivation samples are characterized by a changing matrix composition in the course of the dynamic cultivation progress by the accumulation of analytes and side products, and also by an increasing fluorescence background[33].

To achieve best conditions for monitoring, all measurements were conducted in aluminum microwells. Fig. 2A represents a sketch of the measurement set-up, and the suggested distribution of the Raman signal inside the aluminum microwells, when the focus beam is adjusted just below the fluid surface. The highest scattering intensity is achieved by focusing just beneath the liquid surface[34]. Fig. 2B illustrates the signal enhancement achieved through SERS. Backscattering of the Raman and SERS signal depends on the turbidity of the sample, which follows the Lambert-Beer law[35]. The walls and the bottom of the aluminum microwell are acting as a diffuse reflector for the excited laser emission, as shown in Fig. 2. The aluminum oxide film, which is naturally formed on every Al surface, did not

affect the measurement. According to Zhang et al., anodized aluminum oxide films exhibit weak SERS bands at about 1600 cm^{-1}, which lies outside the spectral range that was evaluated in this study. Bands would occur only if the measurement was tightly focused directly on the Al surface[36]. In common plastic like polystyrene and polyethylene-terephthalate microwell plates, however, significant interference of a strong Raman band at around 1000 cm^{-1} can occur when using a small sampling volume. Al in contrast, if used as material and metallic sample holder, may even act as signal enhancer due to back-reflection[37,38]. Thus, Al seems to be a suitable sample enclosure for a disturbance-reduced Raman and SERS analysis[37,39].

Since the highly concentrated Ag NPs remain stable at the surface during the short measurement process in the microwell (as depicted in Fig. 2B), repeated SERS measurements can be conducted reliably[21] in the same way for each microwell within the given measurement time of the respective Raman techniques used here (cf. Fig. S7).

Fig. 3 summarizes the resulting Raman spectra from both non-SERS measurements (top-row) and SERS-measurements (bottom-row) of the cell-free supernatant samples. As the spectra are presented for the region of interest and offset separated, the impact of fluorescence on NIR- and micro-Raman is not obvious. The highest fluorescence backgrounds are observed with micro-Raman (Fig. 3C and Fig. S7B), which is due to the excitation at 633 nm close to the maximum fluorescence of biological samples. For easier comparison of individual spectra, only a selection is represented. All non-SERS Raman spectra (at the top-row of Fig. 3) show similar Raman bands, but with varying relative intensities with best resolution for TG-Raman. Although TG-Raman excites samples even at the fluorescence maximum of many biological compounds, it seems that the fluorescence is sufficiently reduced and the spectra are clearly distinguishable from the residual background (cf. Fig. 3B and 3E)[6]. Generally, all non-SERS measurements of the three spectroscopic set-ups demonstrate similar results. They appear significantly different from the respective SERS measurements of the supernatant samples (Fig. 3 bottom row).

The detection of analytes with the addition of SERS reveals rather different spectra for the respective Raman technique. The largest differences between enhanced and non-enhanced measurements are

observable from the micro-Raman spectra, with strong variations of the background, spectral peaks and the signal intensity. Overall, the application of SERS using Ag NPs to each sample right before the measurements clearly leads to a better separation of signals from the background noise in the supernatant samples with all Raman techniques (bottom row in Fig. 3D – F). The addition of Ag NPs is revealing further spectral features, which originate from oligonucleotides (678, 730, 925, 1104 and 1330 cm^{-1}, cf. Table 1) like adenosine derivatives (cAMP and AMP), whereas without Ag NPs, mainly compounds of the media substrate such as magnesium sulfate (at 980 cm^{-1}), trace elements and carbohydrates (877-883 cm^{-1} and 1130 cm^{-1}) dominate the Raman spectra[40]. Table 1 shows the observed Raman and SERS peaks related to literature references, and a comparison of detection with the three different techniques.

It is feasible to recognize most changes of substrate and product compounds in the mineral salt medium with all spectroscopic set-ups, but it appears that SERS, in general, provides better resolved spectra (Fig. 3D and 3E). A high effort for adjustment is needed in the case of the microscope set-up (Fig. 3F), yet no distinct peak around 980 cm^{-1} is detectable throughout the course of the cultivation. One reason for this effect may be the smaller focal spot in the sample liquid. Nanoparticles for SERS need to be captured within this tiny spot. The focal spot with the probes used for NIR- and TG-Raman is 10 – 20 fold larger, which likely reduces thresholds, and further results in increased reproducibility of the SERS measurements[41].

Figure 4 shows the development of the concentrations of glucose, acetate, cAMP and AMP during the course of the cultivation measured with the corresponding SERS respectively Raman bands (normalized peak intensities) in comparison to concentrations determined by HPLC. In all cases, a similar development is observed; values of the corresponding quantitative regression analysis are shown in Table 2.

As pulses were applied after a certain time under nutrient-limited fed-batch cultivation conditions, glucose and the concentration of overflow metabolites like acetate varies. This dynamic course is well-captured for glucose and AMP, and at most time points also for cAMP. In case of acetate, which was

only analyzed at samples of non-SERS measurements with NIR-Raman and TG-Raman, general trends were also reflected well, however, with reduced conformity.

Depending on the quality of the spectral data, which were obtained from the three Raman techniques and SERS, different pre-treatments were applied to obtain PLSR models (cf. section 2.6). They appear plausible with respect to the explained variance of calibration and validation, scores, loadings and regression coefficients (Fig. S2, S5 and S6). The spectra obtained from micro-Raman exhibited a high spectral resolution over a wide spectral range, but strong variations of intensities and background, especially for the SERS measurements (cf. Fig. 3C – F), whereas those obtained from NIR-Raman were less resolved with a varying offset. In contrast, TG spectra had only small offsets, well discernable peaks, but a stronger signal to noise ratio. Furthermore, the spectral region was limited to 1000 cm^{-1} in maximum with a poor spectral resolution of the prototype system set-up used here.

In Table 2, a summary of the resulting RMSE for the analytes glucose, acetate, cAMP and AMP is provided for both SERS and non-SERS Raman spectra. The "best" results for each analyte are highlighted in bold, meaning the approach with the smallest RMSE and the least variation among RMSEC-RMSECV and/or the RMSEP. In case of glucose, acetate and cAMP concentrations, indeed non-SERS Raman spectra obtained from the NIR-Raman led to the lowest RMSE. The general ability of non-SERS Raman to monitor glucose and lactate concentration accurately, if compared with 2-D fluorescence and NIR spectroscopy, was recently observed in samples of a cell culture process[42]. A RMSEP of up to 0.31 $g \cdot L^{-1}$ was reported recently[43]. AMP, however, SERS spectra were slightly superior to Raman spectra obtained with the NIR-Raman. To our surprise, for no analyte tested here, the well-resolved microscopic spectra yielded to superior results in quantitative evaluation, but for one analyte, i.e. AMP, quantification even failed. Although nominal low RMSE were obtained for SERS measurements of acetate by micro-Raman, this model fails in cross-validation (cf. supplementary data, Fig. S6A). Moreover, as we observed a nonlinear trend at the upper range of acetate concentrations also in the PLSR model from NIR-Raman spectra (cf. supplementary data, Fig. S6B), we concluded that acetate was not suited for quantitation in the samples used here, since it resulted in high uncertainties for all approaches.

In comparison, for glucose, AMP and cAMP concentrations, low RMSE were achieved, which correspond to relative uncertainties of 8, 5 and 10% in the studied concentration ranges (cf. Fig. S5A-B). From a physiological point of view, the cAMP concentration in *E. coli* increases under limited substrate supply[42,43]. cAMP is an important molecule to indicate the energetic state of a culture and the degree of starvation under typically applied fed-batch conditions, in which the main nutrient is limiting[30]. Due to the oscillating feed rate and various phases of starvation, its concentration increased during the cultivation. The highest peak of cAMP is reached when the ratio of the glucose fed to the residual biomass is at its minimum at 21 h, which is in agreement to observations of Notley-McRobb et al. [42]. While TG-Raman can follow the development of cAMP, NIR-Raman was performing best regarding the quantitative analysis of cAMP (cf. Fig. 4 and Table 2).

The application of SERS had various effects on the spectra. Dominant substrate bands like thiamine (756 cm^{-1}), phosphates (1160 cm^{-1}) and carbohydrates (1130 cm^{-1}) were reduced, while product bands such as lactate (920 cm^{-1}), proteins (around 1220 cm^{-1}), and lipids (1460 cm^{-1}) appear enhanced (cf. Table 1). These results suggest to consider surface-enhanced Raman spectroscopy a reliable approach for the monitoring of metabolites in bioprocesses and make it a promising technology for the refined detection of low-concentrated analytes such as AMP. The combination of such a technology with automated data treatment under the consideration of generic calibration model development[46] can support the suitability of Raman spectroscopy as a valuable process analytical technology for compounds so far difficult to measure in bioprocesses.

4. Conclusion

The motivation for this study was a comparison of different Raman spectroscopic techniques regarding their suitability for the analysis of essential compounds in a bacterial cultivation, namely glucose, acetate, cAMP, and AMP as an indicator of the process status. The comparison was

performed with respect to parallel and/or on-line measurement combined with high sensitivity and robustness. Furthermore, the benefit of a combined SERS approach with each technique was assessed.

In general, both the SERS and the non-SERS spectra of the three set-ups closely resembled each other. Addition of Ag NPs led to an increase of information of Raman active species, at the same time reducing intensities and identifiability of other compounds present in the non-SERS measurements.

Surprisingly, the spectra derived from the most precise instrument, a high-resolution Raman microscope, yielded no superior results for quantitative analysis of any of the observed analytes. Even though producing the best-resolved spectra regarding the number of analytes, SERS added no further benefit for quantitative analysis in this particular study. In contrast, best results in quantitative analysis were obtained from the instrument operating with CW-NIR excitation at 785 nm. Although the signal-to-noise ratio of the Raman peaks seemed poor due to a high fluorescence background, good results were obtained in combination with suitable data transformation and chemometric (PLSR) evaluation. It should be noted that for the quantitative evaluation of the NIR-Raman data MVDA is essential[44]. In case of cAMP, addition of Ag NPs further improved the prediction results from PLSR, however, for glucose, acetate and AMP, no comparable effect was observed with SERS although the spectra exhibited more spectral lines and details[45]. Remarkably, the application of complex media might lead to different conclusions about the benefits of SERS pretreatment and Raman spectroscopy evaluation. Despite the advantages of SERS nanostructures to drastically enhance the Raman signal and quench fluorescence, a careful planned set-up is necessary to carry out reproducible measurement results and neglect effects of signal variations due to aggregation[46,47]. The combination of TG-Raman with SERS is beneficial for a qualitative analysis[48]. In this study, spectra derived from the TG-Raman with and without SERS resulted in well-discernable spectral peaks, which allow the identification of a much higher number of peaks compared to NIR-Raman. Especially this feature makes TG-Raman spectroscopy an important tool for the screening of complex mixtures as they occur in bioprocesses. For the quantitative analysis, however, only the combination with SERS achieved an acceptable accuracy of glucose and acetate concentration measurement.

Acknowledgements

We thank the Academy of Finland, grant agreement no. 1292253 (FOULSENS) and the European Union's Horizon 2020 research and innovation program under the Marie Skłodowska-Curie actions grant agreement no. 643056 (Biorapid) for financial support. We also thank Dr. Oliver Skibitzki and Dipl. Ing. Brigitte Burckhardt for their support during the measurements. The authors gratefully acknowledge the considerable support of Mari Tenhunen and Lauri Kurki, Timegate Instruments Oy, Oulu, Finland, for temporarily providing a TG-Raman instrument and supporting its qualification.

Conflict of Interest

The authors have no conflict of interest.

References

1. Li MY, Ebel B, Paris C, Chauchard F, Guedon E, Marc A. Real-time monitoring of antibody glycosylation site occupancy by in situ Raman spectroscopy during bioreactor CHO cell cultures. *Biotechnol Prog*. 2018. doi:10.1002/btpr.2604.
2. Smith E, Dent G. *Modern Raman Sectroscopy - A Practical Approach*. West Sussex: John Wiley and Sons; 2005.
3. Classen J, Aupert F, Reardon KF, Solle D, Scheper T. Spectroscopic sensors for in-line bioprocess monitoring in research and pharmaceutical industrial application. *Anal Bioanal Chem*. 2016:1-16. doi: 10.1007/s00216-016-0068-x.
4. Lee HLT, Boccazzi P, Gorret N, Ram RJ, Sinskey AJ. *In situ* bioprocess monitoring of *Escherichia coli* bioreactions using Raman spectroscopy. *Vib Spectrosc*. 2004;35(1-2):131-137. doi:10.1016/j.vibspec.2003.12.015.
5. André S, Lagresle S, Hannas Z, Calvosa É, Duponchel L. Mammalian cell culture monitoring using in situ spectroscopy: Is your method really optimised? *Biotechnol Prog*. 2017;33(2):308-316. doi:10.1002/btpr.2430.
6. Rojalin T, Kurki L, Laaksonen T, Viitala T, Kostamovaara J, Gordon KC, Galvis L, Wachsmann-Hogiu S, Strachan CJ, Yliperttula M. Fluorescence-suppressed time-resolved Raman spectroscopy of pharmaceuticals using complementary metal-oxide semiconductor (CMOS) single-photon avalanche diode (SPAD) detector. *Anal Bioanal Chem*. 2016;408(3):761-774. doi: 10.1007/s00216-015-9156-6.
7. Butler HJ, Ashton L, Bird B, Cinque G, Curtis K, Dorney J, Esmonde-white K, Fullwood NJ, Gardner B, Martin-Hirsch PL, Walsh MJ, Mcainsh MR, Stone N, Martin FL. Using Raman spectroscopy to characterise biological materials. *Nat Protoc*. 2016;11(4):664-687. doi: 10.1038/nprot.2016.036.
8. Petry R, Schmitt M, Popp J. Raman spectroscopy--a prospective tool in the life sciences. *Chemphyschem*. 2003;4(1):14-30. doi: 10.1002/cphc.200390004.

9. Wei D, Chen S, Liu Q. Review of Fluorescence Suppression Techniques in Raman Spectroscopy. *Appl Spectrosc Rev*. 2015;50(August 2016):387-406. doi: 10.1080/05704928.2014.999936.

10. Mogilevsky G, Borland L, Brickhouse M, Fountain III AW. Raman Spectroscopy for Homeland Security Applications. *Int J Spectrosc*. 2012;2012:1-12. doi: 10.1155/2012/808079.

11. Sowoidnich K, Kronfeldt HD. Shifted excitation Raman difference spectroscopy at multiple wavelengths for in-situ meat species differentiation. *Appl Phys B Lasers Opt*. 2012;108(4):975-982.

12. De Luca AC, Mazilu M, Riches A, Herrington CS, Dholakia K. Online fluorescence suppression in modulated raman spectroscopy. *Anal Chem*. 2010;82(2):738-745. doi: 10.1021/ac9026737.

13. Song JJ, Eesley GL, Levenson MD. Background suppression in coherent Raman spectroscopy. *Appl Phys Lett*. 1976;29(9):567-569. doi: 10.1063/1.89189.

14. Rodriguez LG, Lockett SJ, Holtom GR. Coherent Anti-Stokes Raman Scattering Microscopy: A Biological Review. *J Int Soc Anal Cytol*. 2006;69(A):659-676. doi: 10.1002/ cyto.a.20299.

15. Smith ZJ, Knorr F, Pagba C V, Wachsmann-Hogiu S. Rejection of fluorescence background in resonance and spontaneous Raman microspectroscopy. *J Vis Exp*. 2011;(51):1-5. doi: 10.3791/2592.

16. Kneipp K, Wang Y, Kneipp H, Perelman LT, Itzkan I. Single molecule detection using surface-enhanced Raman scattering (SERS). *Phys Rev Lett*. 1997;78(9):1667-1670. doi: 10.1103/PhysRevLett.78.1667.

17. Kneipp K, Kneipp H, Itzkan I, Dasari RR, Feld MS. Surface-enhanced non-linear Raman scattering at the single-molecule level. *Chem Phys*. 1999;247:155-162. doi: 10.1016/S0301.

18. Geddes CD. Surface Plasmon Enhanced, Coupled and Controlled Fluorescence. John Wiley & Sons; 2017. doi:10.1002/9781119325161.

19. Cardinal MF, Vander Ende E, Hackler RA, McAnally MO, Stair PC, Schatz GC, Van Duyne RP. Expanding applications of SERS through versatile nanomaterials engineering. *Chem Soc Rev*. 2017;46:3886-3903. doi: 10.1039/C7CS00207F.

20. Kögler M, Zhang B, Cui L, Shi Y, Yliperttula M, Laaksonen T, Viitala T, Zhang K. Real-time Raman based approach for identification of biofouling. *Sensors Actuators, B Chem*. 2016;230:411-421. doi: 10.1016/j.snb.2016.02.079.

21. Strehle KR, Cialla D, Rsch P, Henkel T, Khler M, Popp J, Ro P, Ko M. Article A Reproducible Surface-Enhanced Raman Spectroscopy Approach . Online SERS Measurements in a Segmented Microfluidic System. *Microscopy*. 2007;79(4):1958-1963. doi: 10.1021/ac0615246.

22. McNay G, Eustace D, Smith WE, Faulds K, Graham D. Surface-enhanced Raman scattering (SERS) and surface-enhanced resonance raman scattering (SERRS): A review of applications. *Appl Spectrosc*. 2011;65(8):825-837. doi: 10.1366/11-06365.

23. Kostamovaara J, Tenhunen J, Kögler M, Nissinen I, Nissinen J, Keränen P. Fluorescence suppression in Raman spectroscopy using a time-gated CMOS SPAD. *Opt Express*. 2013. doi:10.1364/OE.21.031632.

24. Uusitalo S, Kögler M, Välimaa A-L, Popov A, Ryabchikov Y, Kontturi V, Siitonen S, Petäjä J, Virtanen T, Laitinen R, Kinnunen M, Meglinski I, Kabashin A, Bunker A, Viitala T, Hiltunen J. Detection of *Listeria innocua* on roll-to-roll produced SERS substrates with gold nanoparticles. *RSC Adv*. 2016;6(67):62981-62989. doi: 10.1039/c6ra08313g.

25. Uusitalo S, Kögler M, Välimaa A-L, Petäjä J, Kontturi V, Siitonen S, Laitinen R, Kinnunen M,

Viitala T, Hiltunen J. Stability optimization of microbial surface-enhanced Raman spectroscopy detection with immunomagnetic separation beads. *Opt Eng*. 2017;56(3):1-7. doi: 10.1117/1.

26. Cui L, Chen P, Chen S, Yuan Z, Yu C, Ren B, Zhang K. *In Situ* Study of the Antibacterial Activity and Mechanism of Action of Silver Nanoparticles by Surface-Enhanced Raman Spectroscopy. *Anal Chem*. 2013;85:5436−5443. doi: 10.1021/ac400245j.

27. Renishaw P. Brochure: inVia confocal Raman microscope. 2017:1. http://www.renishaw.com/en/invia-confocal-raman-microscope--6260.

28. Kaiser Optical Systems I. RXN1 instrument specifications. http://www.kosi.com/na_en/products/raman-spectroscopy/raman-analyzers/raman-rxn1-analyzer.php. Published 2015. Accessed August 10, 2017.

29. Nissinen I, Nissinen J, Keränen P, Kostamovaara J. On the effects of the time gate position and width on the signal-to-noise ratio for detection of Raman spectrum in a time-gated CMOS single-photon avalanche diode based sensor. *Sensors Actuators, B Chem*. 2017;241:1145-1152. doi: 10.1016/j.snb.2016.10.021.

30. Junne S, Klingner A, Kabisch J, Schweder T, Neubauer P. A two-compartment bioreactor system made of commercial parts for bioprocess scale-down studies: Impact of oscillations on *Bacillus subtilis* fed-batch cultivations. *Biotechnol J*. 2011;6(8):1009-1017. doi: 10.1002/biot.201100293.

31. Ryll T, Wagner R. Improved ion-pair high-performance liquid chromatographic method for the quantification of a wide variety of nucleotides and sugar- nucleotides in animal cells. *J Chromatogr*. 1991;570:77-88. doi: 10.1016/0378.

32. Timegate Instruments Oy F. Timegate Instruments Oy products. http://www.timegate.fi/products/. Published 2017. Accessed July 10, 2017.

33. Wilén BM, Onuki M, Hermansson M, Lumley D, Mino T. Microbial community structure in activated sludge floc analysed by fluorescence in situ hybridization and its relation to floc stability. *Water Res*. 2008;42(8-9):2300-2308. doi: 10.1016/j.watres.2007.12.013.

34. Cooney TF, Skinner HT, Angel SM. Comparative study of some fiber-optic remote Raman probe designs. Part I: Model for liquids and transparent solids. *Appl Spectrosc*. 1996;50(7):836-848. doi: 10.1366/0003702963905592.

35. Gordon HR. Can the Lambert-Beer law be applied to the diffuse attenuation coefficient of ocean water? *Limnol Oceanogr*. 1989;34(8):1389-1409. doi:10.4319/lo.1989.34.8.1389.

36. Zhang C, Abdijalilov K, Grebel H. Surface enhanced Raman with anodized aluminum oxide films. *J Chem Phys*. 2007;127(4):044701. doi: 10.1063/1.2752498.

37. Ryder AG, De Vincentis J, Li B, Ryan PW, Sirimuthu NMS, Leister KJ. A stainless steel multi-well plate (SS-MWP) for high-throughput Raman analysis of dilute solutions. *J Raman Spectrosc*. 2010;41(10):1266-1275. doi: 10.1002/jrs.2586.

38. Cui L, Butler HJ, Martin-Hirsch PL, Martin FL. Aluminium foil as a potential substrate for ATR-FTIR, transflection FTIR or Raman spectrochemical analysis of biological specimens. *Anal Methods*. 2016;8(3):481-487. doi: 10.1039/C5AY02638E.

39. Knight MW, King NS, Liu L, Everitt HO, Nordlander P, Halas NJ. Aluminum for plasmonics. *ACS Nano*. 2014;8(1):834-840. doi: 10.1021/nn405495q.

40. Efeoglu E, Culha M. *In situ*-monitoring of biofilm formation by using surface-enhanced raman scattering. *Appl Spectrosc*. 2013;67(5):498-505. doi: 10.1366/12-06896.

41. Lewis IR, Griffiths PR. Raman spectrometry with fiber-optic sampling. *Appl Spectrosc*.

1996;50(10). doi:10.1366/0003702963904908.

42. Rowland-Jones RC, van den Berg F, Racher AJ, Martin EB, Jaques C. Comparison of spectroscopy technologies for improved monitoring of cell culture processes in miniature bioreactors. *Biotechnol Prog*. 2017;33(2):337-346. doi:10.1002/btpr.2459.

43. Santos RM, Kessler J-M, Salou P, Menezes JC, Peinado A. Monitoring mAb Cultivations with In-Situ Raman Spectroscopy: The influence of spectral selectivity on calibration models and industrial use as reliable PAT Tool. *Biotechnol Prog*. 2018:1-12. doi:10.1002/btpr.2635.

44. Notley-McRobb L, Death A, Ferenci T. The relationship between external glucose concentration and cAMP levels inside. *Biochem J*. 2006;(1997):1909-1918. doi: 10.1099/00221287-143-6-1909.

45. Lin H, Hoffmann F, Rozkov A, Enfors SO, Rinas U, Neubauer P. Change of extracellular cAMP concentration is a sensitive reporter for bacterial fitness in high-cell-density cultures of *Escherichia coli*. *Biotechnol Bioeng*. 2004;87(5):602-613. doi: 10.1002/bit.20152.

46. Webster TA, Hadley BC, Hilliard W, Jaques C, Mason C. Development of Generic Raman Models for a GS-KOTM CHO Platform Process. *Biotechnol Prog*. 2018. doi: 10.1002/btpr.2633.

47. Kämmer E, Olschewski K, Stöckel S, Rösch P, Weber K, Cialla-May D, Bocklitz T, Popp J. Quantitative SERS studies by combining LOC-SERS with the standard addition method. *Anal Bioanal Chem*. 2015;407(29):8925-8929. doi: 10.1007/s00216-015-9045-z.

48. Kögler M, Ryabchikov YV, Uusitalo S, Popov A, Popov A, Tselikov G, Välimaa A-L, Al-Kattan A, Hiltunen J, Laitinen R, Neubauer P, Meglinski I, Kabashin A. Bare laser-synthesized Au-based nanoparticles as non-disturbing SERS probes for Bacteria Identification. *Journal of biophotonics*. 2018. doi:10.1002/jbio.201700225

49. Makino R, Obayashi E, Homma N, Shiro Y, Hori H. YC-1 facilitates release of the proximal his residue in the NO and CO complexes of soluble guanylate cyclase. *J Biol Chem*. 2003;278(13):11130-11137. doi: 10.1074/jbc.

50. Cui L, Chen P, Zhang B, Zhang D, Li J, Martin FL, Zhang K. Interrogating chemical variation via layer-by-layer SERS during biofouling and cleaning of nanofiltration membranes with further investigations into cleaning efficiency. *Water Res*. 2015;87:282-291. doi: 10.1016/j.watres.2015.09.037.

51. Green M, Liu FM, Cohen L, Kollensperger P, Cass T. SERS platforms for high density DNA arrays. *Faraday Discuss*. 2006;132:269-319. doi: 10.1039/B506636K.

52. Kubryk P, Niessner R, Ivleva NP. The origin of the band at around 730 cm(-1) in the SERS spectra of bacteria: a stable isotope approach. *Analyst*. 2016;141(10):2874-2878. doi: 10.1039/c6an00306k.

53. Premasiri WR, Lee JC, Sauer-Budge A, Theberge R, Costello CE, Ziegler LD. The biochemical origins of the surface-enhanced Raman spectra of bacteria: a metabolomics profiling by SERS. *Anal Bioanal Chem*. 2016:1-17. doi: 10.1007/s00216-016-9540-x.

54. Leopold N, Cîntă-Pînzaru S, Baia M, Antonescu E, Cozar O, Kiefer W, Popp J. Raman and surface-enhanced Raman study of thiamine at different pH values. *Vib Spectrosc*. 2005;39(2):169-176. doi:10.1016/j.vibspec.2005.02.019.

55. Uusitalo S, Popov A, Ryabchikov Y V., Bibikova O, Alakomi HL, Juvonen R, Kontturi V, Siitonen S, Kabashin A, Meglinski I, Hiltunen J, Laitila A. Surface-enhanced Raman spectroscopy for identification and discrimination of beverage spoilage yeasts using patterned substrates and gold nanoparticles. *J Food Eng*. 2017:1-8. doi: 10.1016/j.jfoodeng.2017.05.007.

56. Efeoglu E, Culha M. Surface-Enhanced Raman Scattering for Biofilm Characterization.

Spectroscopy. 2013;28(11):36-41. doi: 10.3390/chemosensors6010005.

57. Witkowska E, Korsak D, Kowalska A, Księżopolska-Gocalska M, Niedziółka-Jönsson J, Roźniecka E, Michałowicz W, Albrycht P, Podrażka M, Hołyst R, Waluk J, Kamińska A. Surface-enhanced Raman spectroscopy introduced into the International Standard Organization (ISO) regulations as an alternative method for detection and identification of pathogens in the food industry. *Anal Bioanal Chem*. 2017;409(6):1555-1567. doi: 10.1007/s00216-016-0090-z.

58. Cui L, Yang K, Zhou G, Huang WE, Zhu Y. Surface-Enhanced Raman Spectroscopy Combined with Stable Isotope Probing to Monitor Nitrogen Assimilation at Both Bulk and Single-Cell Level. 2017;11(89):5793-5800. doi:10.1021/acs.analchem.6b04913.

59. Narayanan PS. Raman spectrum of potassium di-hydrogen phosphate. *Proc Indian Acad Sci - Sect A*. 1951;33(4):240-244. doi: 10.1007/BF03039052.

60. Fan C, Hu Z, Mustapha A, Lin M. Rapid detection of food- and waterborne bacteria using surface-enhanced Raman spectroscopy coupled with silver nanosubstrates. *Appl Microbiol Biotechnol*. 2011;92(5):1053-1061. doi: 10.1007/s00253-011-3634-3.

61. Moody AS, Baghernejad PC, Webb KR, Sharma B. Surface Enhanced Spatially Offset Raman Spectroscopy Detection of Neurochemicals Through the Skull. *Anal Chem*. 2017;89:5688-5692. doi: 10.1021/acs.analchem.7b00985.

62. Hampton C, Demoin D. Vibrational Spectroscopy Tutorial: Sulfur and phosphorus. https://faculty.missouri.edu/~glaserr/8160f10/A03_Silver.pdf. Published 2010. Accessed July 12, 2017.

63. David C. Raman Spectroscopy for proteins. Raman Spectroscopy. http://www.horiba.com/fileadmin/uploads/Scientific/Documents/Raman/HORIBA_webinar_proteins.pdf. Published 2012. Accessed July 13, 2017.

64. Walter A, Reinicke M, Bocklitz T, Schumacher W, Rösch P, Kothe E, Popp J. Raman spectroscopic detection of physiology changes in plasmid-bearing *Escherichia coli* with and without antibiotic treatment. *Anal Bioanal Chem*. 2011;400(9):2763-2773. doi: 10.1021/acs.analchem.7b00985.

Figures

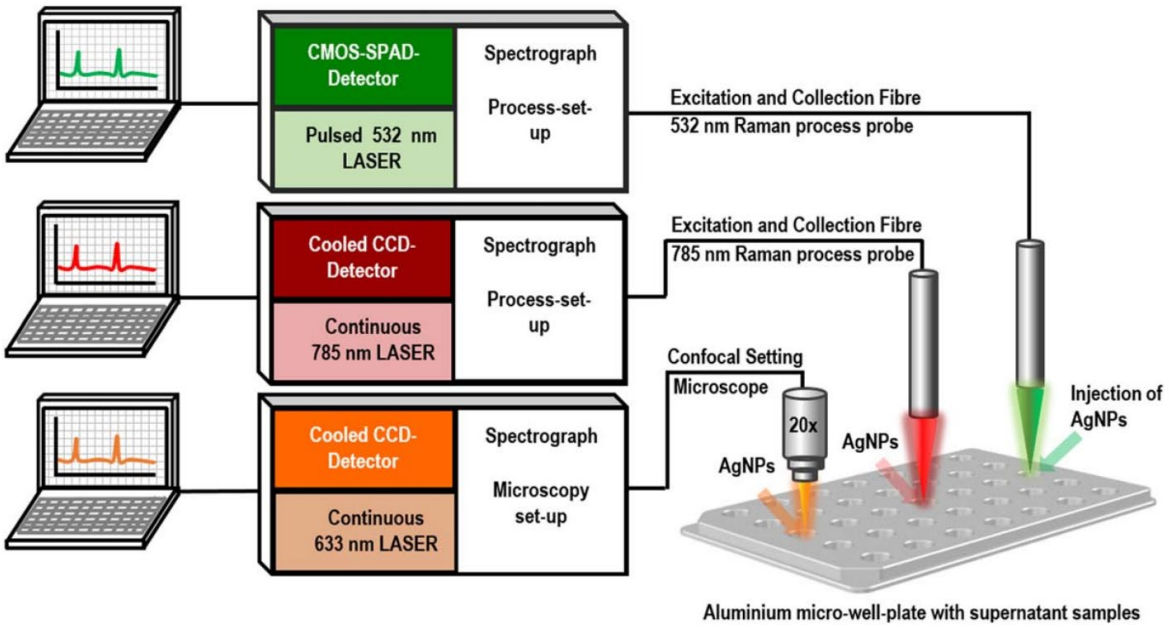

Figure 1

Various spectroscopic set-ups: TG-Raman (TGM1) with pulsed green λ = 532 nm laser, NIR-Raman (RXN1) with red λ = 785 nm laser and confocal setting of micro-Raman (InVia) with orange λ = 633 nm laser used in this work; each measurement without and with injection of Ag NPs into each microwell.

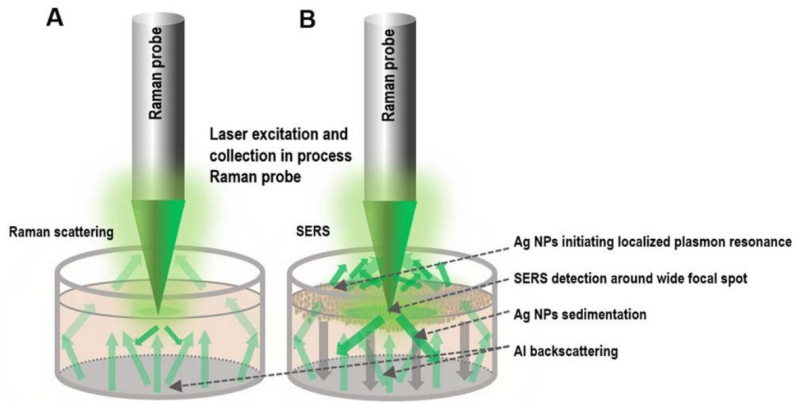

Figure 2

Microwell with supernatant sample - symbolical representation of scattering (A) Raman set-up and (B) SERS set-up during measurements in a single aluminum well.

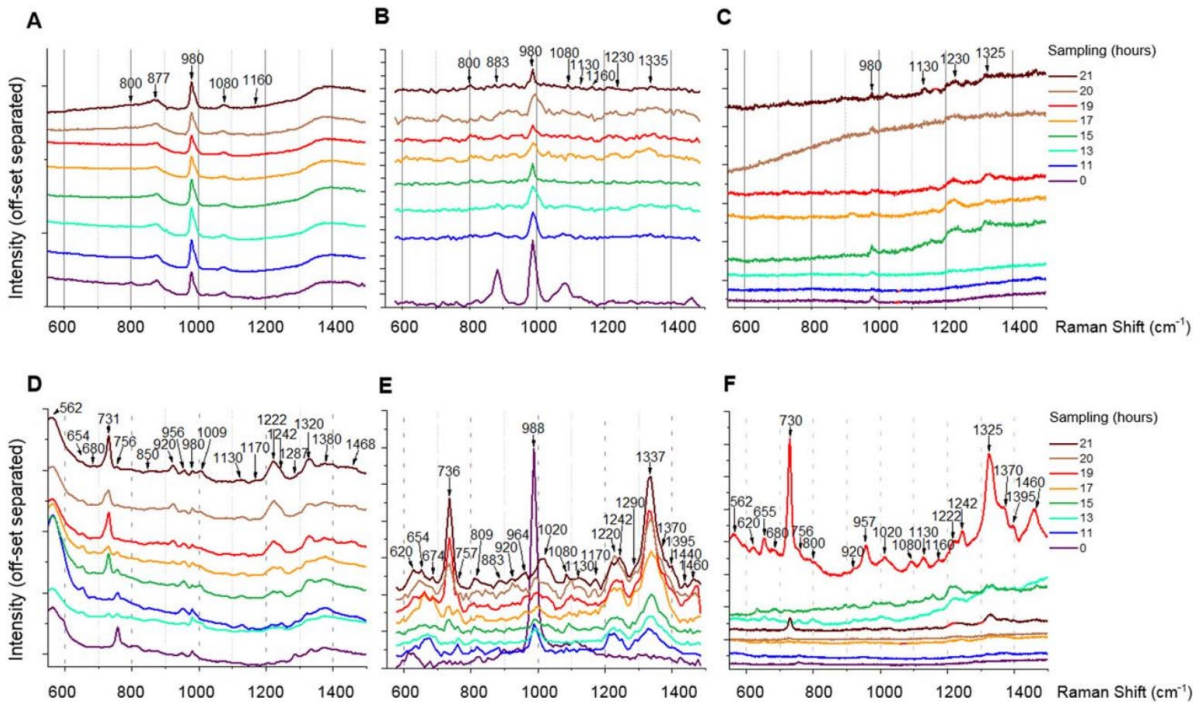

Figure 3

Raman spectra as obtained with NIR-, TG- and micro-Raman (A–C) and spectra from same techniques using SERS (D-F).

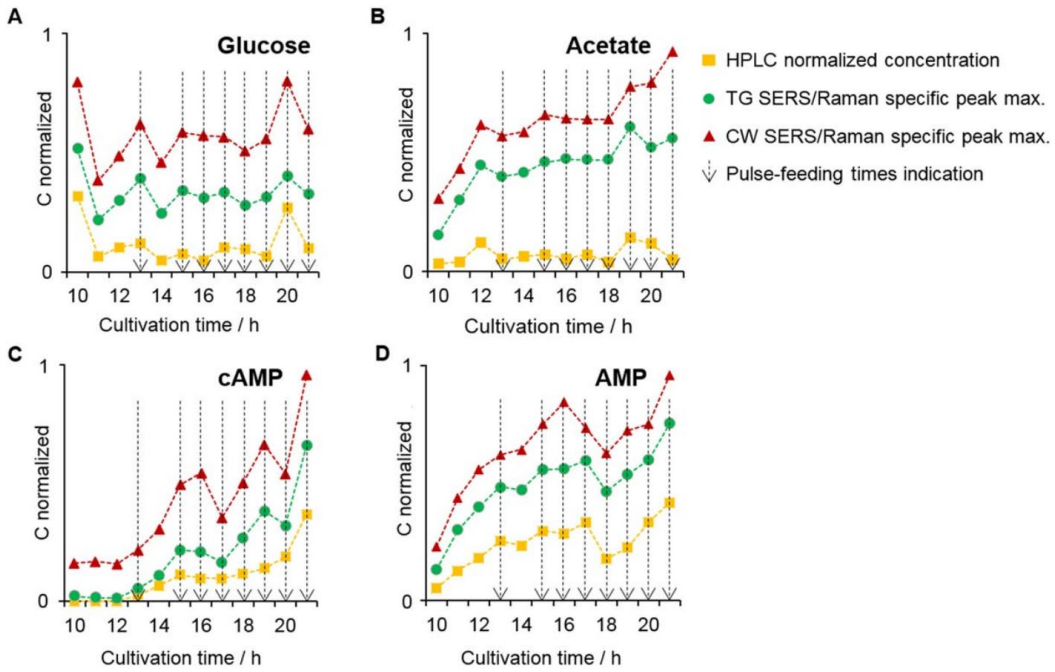

Figure 4

Normalized (0-1) concentrations of A) glucose (1130 cm^{-1}), B) acetate (877–891 cm^{-1}), C) cAMP (731–736 cm^{-1}), and D) AMP (1320–1340 cm^{-1}), corresponding max. peak height measured by NIR-Raman (red triangles) and TG-Raman (green dots) in SERS mode except for acetate (Raman max. peaks). The yellow curve with squares refers to the actual HPLC concentration in mM per sample during the cultivation.

Table 1

Tentative Raman/SERS band assignments with different spectroscopic settings

Detected Bands *Peak/cm^{-1}*	***Tentative band assignment***	***Origin/category***	***Raman*** *NIR-Raman*	***Raman*** *Micro-Raman*	***Raman*** *TG-Raman*	***SERS*** *NIR-Raman*	***SERS*** *Micro-Raman*	***SERS*** *TG-Raman*	***Reference***
562-580	Ring and CH-deformation	Carbohydrate in medium	-	-	-	+	+	ND	[49]
655	Ring breathing of Guanine (oligo G)	DNA	-	-	-	+	+	+	[50]
674-680	Ring breathing of Guanine (oligo G)	DNA	-	-	-	+	+	+	[51]
732-736	Glycosidic ring mode of D-glucosamine (NAG), Adenine or CH_2, cAMP	DNA, Nucleotide	-	-	-	+	+	+	[52] [53]
756	Thiamine	Substrate from medium	-	-	-	+	+	+	[54]
800-810	Acetate (weak peak TG-Raman w. SERS)	Product	+	-	-	-	+	+	this work
877-891	Acetate (weak peak in NIR-Raman)	Product	+	+	+	-	-	-	this work
920	C-C stretch of proline ring-glucose or lactic acid	Product	-	-	-	+	+	+	[55,56,4]
957-964	C=C deformation, guanine	DNA	-	-	-	+	+	+	[57]
1025	C−H bending	Lipid	-	-	-	-	+	+	[58]
1080	Potassium di-hydrogen phosphate	Phosphates in medium	+	+	+	-	+	+	[59]
1130	C–N and C–C stretch	Carbohydrate in medium	-	-	-	+	+	+	[60]
1160	C−O−C or P=O stretch	Phosphates in medium	+	-	+	-	-	-	[61,62]
1170	Tryptophan (Trp) or phenylalanine (Phe)	Aromatic amino acids	-	-	-	+	+	+	[63]
1320-1340	Adenine (AMP)	DNA, Nucleotide	-	-	-	+	+	+	[50] [64]

Table 2

Prediction of analyte concentrations based on Raman and SERS measurements (numbers in brackets refer to factors in PLSR as obtained by cross validation)

Raman technique		**micro-Raman (Renishaw inVia)**			**NIR-process Raman (RXN1)**			**TG-Raman (TGM1)**	
Data pre-treatment for PLSR		1st derivative, S-G smoothing, 2nd order polynomial, 21 wavenumbers, unit vector normalization			1st derivative, S-G smoothing, 2nd order polynomial, 31 wavenumbers, unit vector normalization			Baseline correction, unit vector normalization	
Analyte / conc. Range	**Sample**	**RMSEC**	**RMSECV**	**RMSEP**	**RMSEC**	**RMSECV**	**RMSEP**	**RMSEC**	**RMSECV**
Glucose / g L^{-1}	Raman	0.69	0.78 (1)	1.03 (1)	**0.42**	**0.52 (3)**	**0.39 (3)**	0.75	1.42 (2)
Range: 0.065 – 5.00	SERS	0.57	0.68 (2)	0.57 (4)	0.54	0.61 (1)	0.91	0.70	1.01 (2)
Acetate / g L^{-1}	Raman	0.07	0.09 (3)	n.d.	**0.07**	**0.09 (2)**	**0.08 (4)**	n.d.	n.d.
Range: 0– 0.56	SERS	0.06	0.08 (4)	0.14 (3)	n.d.	n.d.	n.d.	0.12	0.19 (2)
AMP / mM	Raman	n.d.	n.d.	n.d.	0.005	0.01	0.02	n.d.	n.d.
Range: 0– 0.19	SERS	n.d.	n.d.	n.d.	**0.003**	**0.01 (4)**	**0.01 (4)**	n.d.	n.d.
cAMP / mM	Raman	0.02	0.05 (3)	0.06 (3)	**0.01**	**0.02 (4)**	**0.05 (3)**	n.d.	n.d.
Range: 0– 0.51	SERS	0.04	0.06 (3)	0.07 (3)	0.04	0.05 (1)	0.07 (4)	n.d.	n.d.